ELSEVIER

Nuclear Physics A 686 (2001) 141–162

NUCLEAR PHYSICS A

www.elsevier.nl/locate/npe

Projected shell model study for the yrast-band structure of the proton-rich mass-80 nuclei

R. Palit [a,*], J.A. Sheikh [a,b], Y. Sun [c,d], H.C. Jain [a]

[a] *Tata Institute of Fundamental Research, Mumbai 400 005, India*
[b] *Physik-Department, Technische Universität München, D-85747 Garching, Germany*
[c] *Department of Physics and Astronomy, University of Tennessee, Knoxville, TN 37996, USA*
[d] *Department of Physics, Xuzhou Normal University, Xuzhou, Jiangsu 221009, PR China*

Received 27 June 2000; revised 11 September 2000; accepted 10 October 2000

Abstract

A systematic study of the yrast-band structure for the proton-rich, even–even mass-80 nuclei is carried out using the projected shell model approach. We describe the energy spectra, transition quadrupole moments and gyromagnetic factors. The observed variations in energy spectra and transition quadrupole moments in this mass region are discussed in terms of the configuration mixing of the projected deformed Nilsson states as a function of shell filling. © 2001 Elsevier Science B.V. All rights reserved.

PACS: 21.60.Cs; 21.10.Ky; 21.10.Re; 27.50.+e
Keywords: Quadrupole pairing interaction; Transition quadrupole moments; Multi-quasiparticle states; Band-crossings

1. Introduction

The study of low- and high-spin phenomena in the proton-rich mass-80 nuclei have attracted considerable interest in recent years. This has been motivated by the increasing power of experimental facilities and improved theoretical descriptions, as well as by the astrophysical requirement in understanding the structure of these unstable nuclei. In comparison to the rare-earth region where the change in nuclear structure properties is quite smooth with respect to particle number, the structure of the proton-rich mass-80 nuclei shows considerable variations when going from one nucleus to another. This is mainly due to the fact that the available shell model configuration space in the mass-80 region is much smaller than in the rare-earth region. The low single-particle level density implies that

* Corresponding author.
E-mail address: palit@tifr.res.in (R. Palit).

0375-9474/01/$ – see front matter © 2001 Elsevier Science B.V. All rights reserved.
PII: S0375-9474(00)00509-1

a drastic change near the Fermi surfaces can occur among neighboring nuclei. Another fact is that in these medium-mass proton-rich nuclei, neutrons and protons occupy the same single-particle orbits. As the nucleus rotates, pair alignments of neutrons and protons compete with each other and in certain circumstances they can align simultaneously.

Thanks to the new experimental facilities, in particular, to the newly constructed detector arrays, the domain of nuclides accessible for spectroscopic studies has increased drastically during the past decade. For example, some extensive measurements [1–10] of the transition quadrupole-moments, extracted from the level lifetimes and excitation energy of 2^+ state, have been carried out for Kr-, Sr- and Zr-isotopes. These measurements have revealed large variations in nuclear structure of these isotopes with respect to particle number and angular momentum. It has been shown that alignment of proton- and neutron-pairs at higher angular momenta can change the nuclear shape from prolate to triaxial and to oblate.

A systematic description for all these observations poses a great challenge to theoretical models. The early mean-field approaches were devoted to a general study of the structure in the mass-80 region. Besides the work using the Woods–Saxon approach [11], there were studies using the Nilsson model [12] and the Skyrme Hartree–Fock + BCS theory [13]. More recently, microscopic calculations were performed using the Excited VAMPIR approach [14,15]. However, this approach is numerically quite involved and is usually employed to study some quantities for selected nuclei. The large-scale spherical shell model diagonalization calculations [16] have been recently successful in describing the pf-shell nuclei, but the configuration space required for studying the well-deformed mass-80 nuclei is far beyond what the modern computers can handle.

Recently, the projected shell model (PSM) [17] has become quite popular to study the structure of deformed nuclei. The advantage in this method is that the numerical requirement is minimal and, therefore, it is possible to perform a systematic study for a group of nuclei in a reasonable time frame. The PSM approach is based on the diagonalization in the angular-momentum projected basis from the deformed Nilsson states. A systematic study of the rare-earth nuclei [18,19] has been carried out and the agreement between the PSM results and experimental data has been found to be quite good. Very recently, the PSM approach has also been used to study the high-spin properties of ^{74}Se [20], which lies in the mass-80 region.

The purpose of the present work is to perform a systematic PSM study of the low- and high-spin properties for the proton-rich, even–even Kr-, Sr- and Zr-isotopes. The physical quantities to be described are energy spectrum, transition quadrupole moment and gyromagnetic factor. In addition, to compare the available data with theory in a systematic way, we also make predictions for the structure of the $N = Z$ nuclei which could be tested by future experiments with radioactive ion beams. We shall begin our discussion with an outline of the PSM in Section 2. The results of calculations and comparisons with experimental data are presented in Section 3. Finally, the conclusions are given in Section 4.

2. The projected shell model

In this section, we shall briefly outline the basic philosophy of the PSM. For more details about the model, the reader is referred to the review article [17]. The PSM is based on the spherical shell model concept. It differs from the conventional shell model in that the PSM uses the angular momentum projected states as the basis for the diagonalization of the shell model Hamiltonian. What one gains by starting from a deformed basis is not only that shell model calculations for heavy nuclei become feasible but also physical interpretation for the complex systems becomes easier and clearer.

The wave function in the PSM is given by

$$|\sigma, IM\rangle = \sum_{K,\kappa} f_{\kappa}^{\sigma} \widehat{P}^{I}_{MK} |\phi_{\kappa}\rangle. \tag{1}$$

The index σ labels the states with same angular momentum and κ the basis states. $\widehat{P}^{I}_{MK}$ is angular momentum projection operator and f_{κ}^{σ} are the weights of the basis states κ.

We have assumed axial-symmetry for the basis states and the intrinsic states are, therefore, the eigenstates of the K-quantum number. For calculations of an even–even system, the following four kinds of basis states $|\phi_{\kappa}\rangle$ are considered: the quasiparticle (qp) vacuum $|0\rangle$, two-quasineutron states $a^{\dagger}_{\nu_1} a^{\dagger}_{\nu_2}|0\rangle$, two-quasiproton states $a^{\dagger}_{\pi_1} a^{\dagger}_{\pi_2}|0\rangle$, and two-quasineutron plus two-quasiproton (or 4-qp) states $a^{\dagger}_{\nu_1} a^{\dagger}_{\nu_2} a^{\dagger}_{\pi_1} a^{\dagger}_{\pi_2}|0\rangle$. The projected vacuum $|0\rangle$, for instance, is the ground-state band (g-band) of an even–even nucleus.

The weight factors, f_{κ}^{σ} in Eq. (1), are determined by diagonalization of the shell model Hamiltonian in the space spanned by the projected basis states given above. This leads to the eigenvalue equation

$$\sum_{\kappa'} (H_{\kappa\kappa'} - E_{\sigma} N_{\kappa\kappa'}) f_{\kappa'}^{\sigma} = 0, \tag{2}$$

and the normalization is chosen such that

$$\sum_{\kappa\kappa'} f_{\kappa}^{\sigma} N_{\kappa\kappa'} f_{\kappa'}^{\sigma'} = \delta_{\sigma\sigma'}, \tag{3}$$

where the Hamiltonian and norm-matrix elements are given by

$$H_{\kappa\kappa'} = \langle\phi_{\kappa}|\widehat{H}\widehat{P}^{I}_{K_{\kappa}K_{\kappa'}}|\phi_{\kappa'}\rangle, \tag{4}$$

$$N_{\kappa\kappa'} = \langle\phi_{\kappa}|\widehat{P}^{I}_{K_{\kappa}K_{\kappa'}}|\phi_{\kappa'}\rangle. \tag{5}$$

In the numerical calculations, we have used the standard quadrupole–quadrupole plus (monopole and quadrupole) pairing force, i.e.,

$$\widehat{H} = \widehat{H}_0 - \frac{1}{2}\chi \sum_{\mu} \widehat{Q}^{\dagger}_{\mu} \widehat{Q}_{\mu} - G_{\mathrm{M}} \widehat{P}^{\dagger} \widehat{P} - G_{\mathrm{Q}} \sum_{\mu} \widehat{P}^{\dagger}_{\mu} \widehat{P}_{\mu}, \tag{6}$$

where $\widehat{H}_0$ is the spherical single-particle Hamiltonian. The strength of the quadrupole force χ is adjusted such that the known quadrupole deformation parameter ϵ_2 is obtained. This

condition results from the mean-field approximation of the quadrupole–quadrupole interaction of the Hamiltonian in Eq. (6). The monopole pairing force constants $G_{\rm M}$ are adjusted to give the known energy gaps. For all the calculations in this paper, we have used [20]

$$G_{\rm M}^{\nu} = \left[20.25 - 16.20\frac{N-Z}{A}\right]A^{-1}, \qquad G_{\rm M}^{\pi} = 20.25A^{-1}. \tag{7}$$

The strength parameter $G_{\rm Q}$ for quadrupole pairing is assumed to be proportional to $G_{\rm M}$. It has been shown that the band crossing spins vary with the magnitude of the quadrupole pairing force [21]. The ratio $G_{\rm Q}/G_{\rm M}$ ($\equiv \gamma$) can therefore be adjusted to reproduce the observed band crossings and the value of γ used for each nuclei are given in Table 1.

Electromagnetic transitions can give important information on the nuclear structure and provide a stringent test of a particular model. In the present work, we have calculated the electromagnetic properties using the PSM approach. The reduced transition probabilities B(EL) from the initial state $(\sigma_{\rm i}, I_{\rm i})$ to the final state $(\sigma_{\rm f}, I_{\rm f})$ are given by [19]

$$B(\mathrm{EL}, I_{\rm i} \to I_{\rm f}) = \frac{e^2}{(2I_{\rm i}+1)}\left|\langle\sigma_{\rm f}, I_{\rm f}\|\widehat{Q}_L\|\sigma_{\rm i}, I_{\rm i}\rangle\right|^2, \tag{8}$$

where the reduced matrix element is given by

$$\begin{aligned}
&\langle\sigma_{\rm f}, I_{\rm f}\|\widehat{Q}_L\|\sigma_{\rm i}, I_{\rm i}\rangle \\
&\quad= \sum_{\kappa_{\rm i},\kappa_{\rm f}} f_{\kappa_{\rm i}}^{\sigma_{\rm i}} f_{\kappa_{\rm f}}^{\sigma_{\rm f}} \sum_{M_{\rm i},M_{\rm f},M} (-)^{I_{\rm f}-M_{\rm f}} \begin{pmatrix} I_{\rm f} & L & I_{\rm i} \\ -M_{\rm f} & M & M_{\rm i}\end{pmatrix} \langle\phi_{\kappa_{\rm f}}|\widehat{P}^{I_{\rm f}}_{K_{\kappa_{\rm f}}M_{\rm f}}\widehat{Q}_{LM}\widehat{P}^{I_{\rm i}}_{K_{\kappa_{\rm i}}M_{\rm i}}|\phi_{\kappa_{\rm i}}\rangle \\
&\quad= 2\sum_{\kappa_{\rm i},\kappa_{\rm f}} f_{\kappa_{\rm i}}^{\sigma_{\rm i}} f_{\kappa_{\rm f}}^{\sigma_{\rm f}} \sum_{M',M''} (-)^{I_{\rm f}-K_{\kappa_{\rm f}}}(2I_{\rm f}+1)^{-1} \begin{pmatrix} I_{\rm f} & L & I_{\rm i} \\ -K_{\kappa_{\rm f}} & M' & M''\end{pmatrix} \\
&\qquad\qquad \times \int \mathrm{d}\Omega\, D_{M''K_{\kappa_{\rm i}}}(\Omega)\langle\phi_{\kappa_{\rm f}}|\widehat{Q}_{LM'}\widehat{R}(\Omega)|\phi_{\kappa_{\rm i}}\rangle.
\end{aligned} \tag{9}$$

Table 1
Deformation and quadrupole pairing strengths used in PSM calculations

Nuclei	ϵ_2	$\gamma \equiv G_{\rm Q}/G_{\rm M}$
Prolate deformation		
^{72}Kr	0.36	0.16
^{74}Kr	0.37	0.16
^{76}Kr	0.36	0.24
^{76}Sr	0.36	0.16
^{78}Sr	0.36	0.16
^{80}Sr	0.34	0.16
^{80}Zr	0.36	0.16
^{82}Zr	0.29	0.16
^{84}Zr	0.22	0.16
Oblate deformation		
^{68}Se	−0.26	0.16
^{74}Kr	−0.24	0.16

The transition quadrupole moment $Q_t(I)$ is related to the $B(E2)$ transition probability through

$$Q_t(I) = \left(\frac{16\pi}{5} \frac{B(E2, I \to I-2)}{\langle IK20|I-2K\rangle} \right)^{1/2}. \tag{10}$$

In the calculations, we have used the effective charges of $1.5e$ for protons and $0.5e$ for neutrons, which are the same as in the previous PSM calculations [17,19].

Variation of Q_t with spin I can provide information on shape evolution in nuclei. In the case of a rigid rotor, the Q_t curve as a function of I is a straight line. Experimentally, one finds a deviation from the rigid body behavior for most of the nuclei in this mass region. One expects more or less a constant value in Q_t up to the first band crossing. At the band crossing, one often sees a dip in Q_t value due to a small overlap between the wave functions of the initial and the final states involved. There can be a change in Q_t values after the first band crossing, which indicates a shape change induced by quasiparticle alignment.

The other important electromagnetic quantity, which can give crucial information about the level occupancy and thus is an direct indication of the nature of alignment, is the gyromagnetic factor (g-factor). The g-factors $g(\sigma, I)$, $g_\pi(\sigma, I)$ and $g_\nu(\sigma, I)$ are defined by [19]

$$g(\sigma, I) = \frac{\mu(\sigma, I)}{\mu_N I} = g_\pi(\sigma, I) + g_\nu(\sigma, I), \tag{11}$$

with $g_\tau(\sigma, I)$, $\tau = \pi, \nu$ given by

$$\begin{aligned} g_\tau(\sigma, I) \;=\; & \frac{1}{\mu_N [I(I+1)]^{1/2}} \\ & \times \left[g_l^\tau \langle \sigma, I \| \hat{J}^\tau \| \sigma, I \rangle + (g_s^\tau - g_l^\tau) \langle \sigma, I \| \widehat{S}^\tau \| \sigma, I \rangle \right], \end{aligned} \tag{12}$$

and $\mu(\sigma, I)$ is the magnetic moment of a state (σ, I). In our calculations, the following standard values of g_l and g_s have been taken: $g_l^\pi = 1$, $g_l^\nu = 0$, $g_s^\pi = 5.586 \times 0.75$ and $g_s^\nu = -3.826 \times 0.75$. Unfortunately, very few experiments [22–24] have been done to measure the g-factors in this mass region. The only experiment which has recently been performed is for ^{84}Zr [24]. In the present paper, we have calculated g-factors for this nucleus and compared with the data.

3. Results and discussions

The PSM calculations proceed in two steps. In the first step, an optimum set of deformed basis is constructed from the standard Nilsson potential. The Nilsson parameters are taken from Ref. [27] and the calculations are performed by considering three major shells ($N = 2$, 3 and 4) for both protons and neutrons. The basis deformation ϵ_2 used for each nucleus is taken either from experiment if measurement has been done or from the theoretical value of the total Routhian surface (TRS) calculations. Their values are listed in Table 1. The intrinsic states within an energy window of 3.5 MeV around the Fermi surface are considered. This gives rise to the size of the basis space, $|\phi_\kappa\rangle$ in Eq. (1), of the order

of 40. In the second step, these basis states are projected to good angular-momentum states, and the projected basis is then used to diagonalize the shell model Hamiltonian. The detailed calculations have been carried out for Kr-, Sr- and Zr-isotopes and the results are discussed in the following subsections. The band diagram [18], which gives the projected energies for the configurations close to the Fermi surface is shown in Figs. 1–3

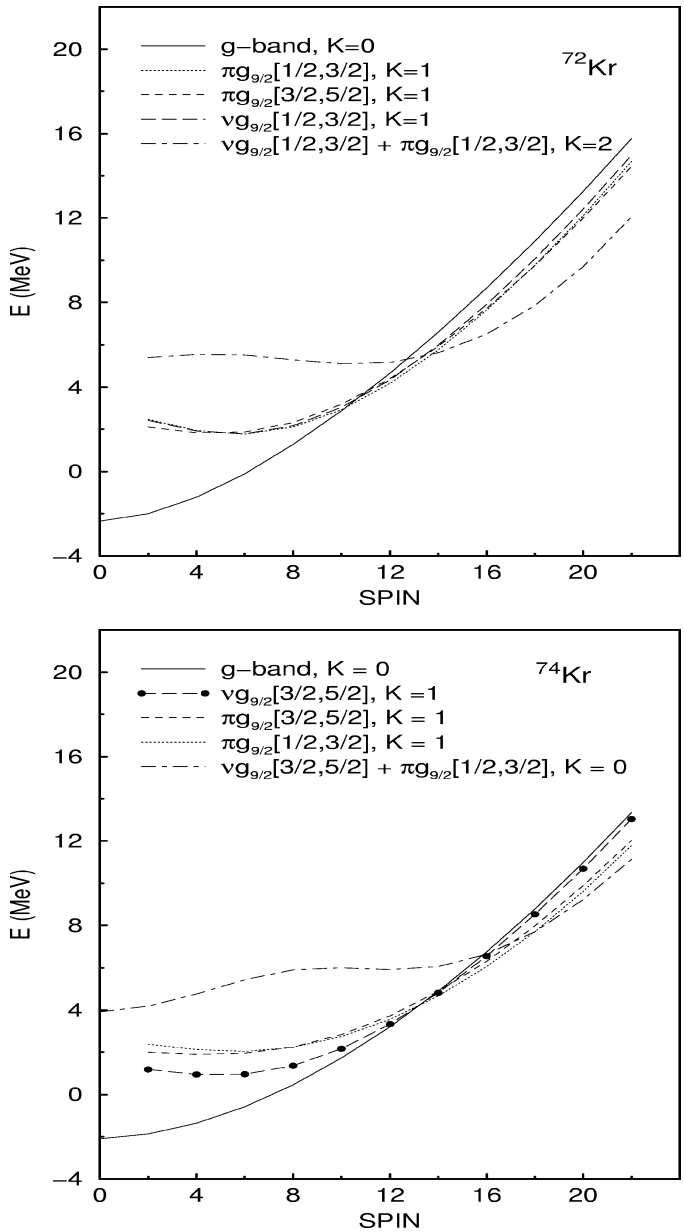

Fig. 1. Band diagrams for Kr isotopes.

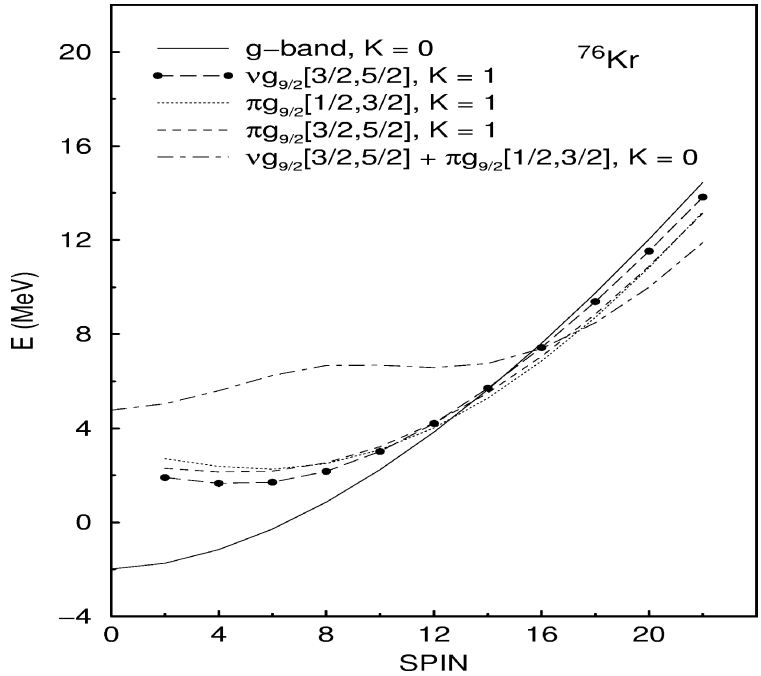

Fig. 1. —continued.

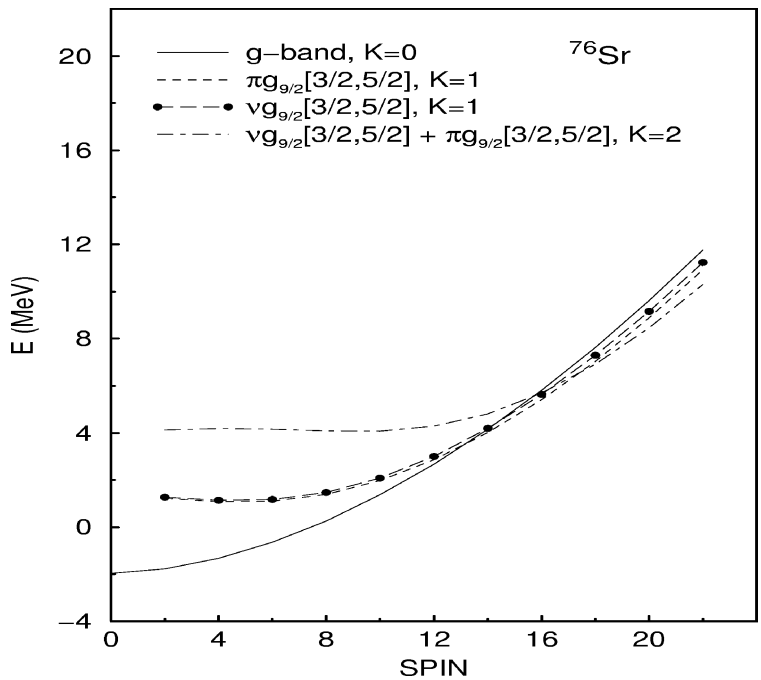

Fig. 2. Band diagrams for Sr isotopes.

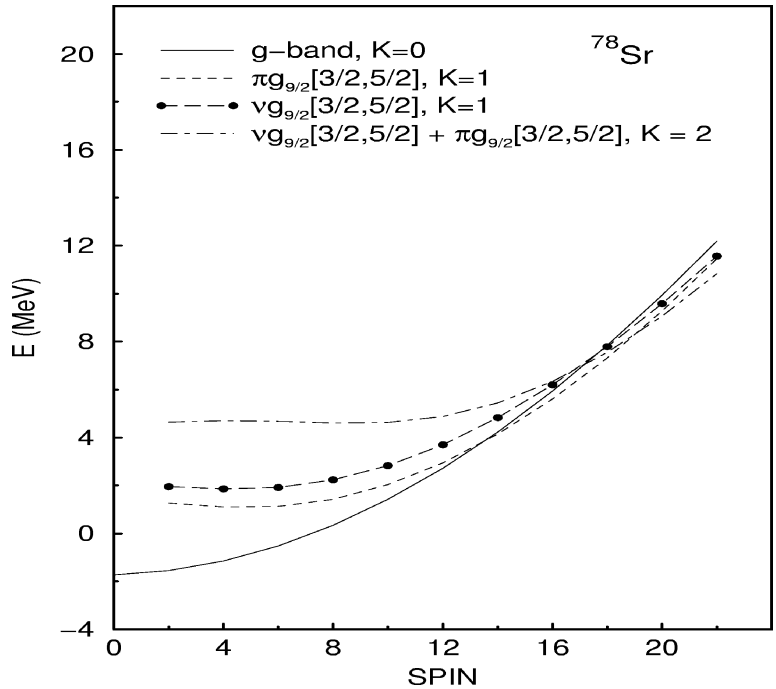

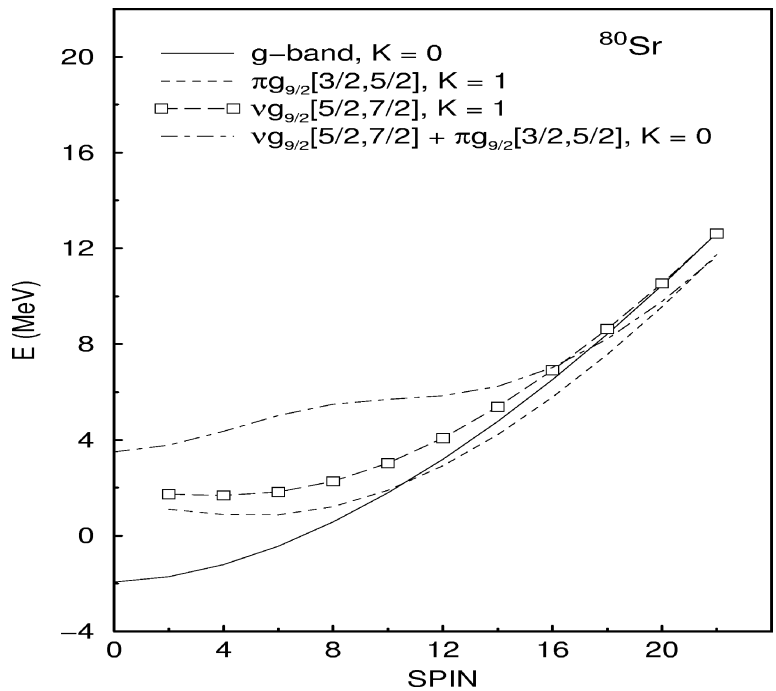

Fig. 2. —continued.

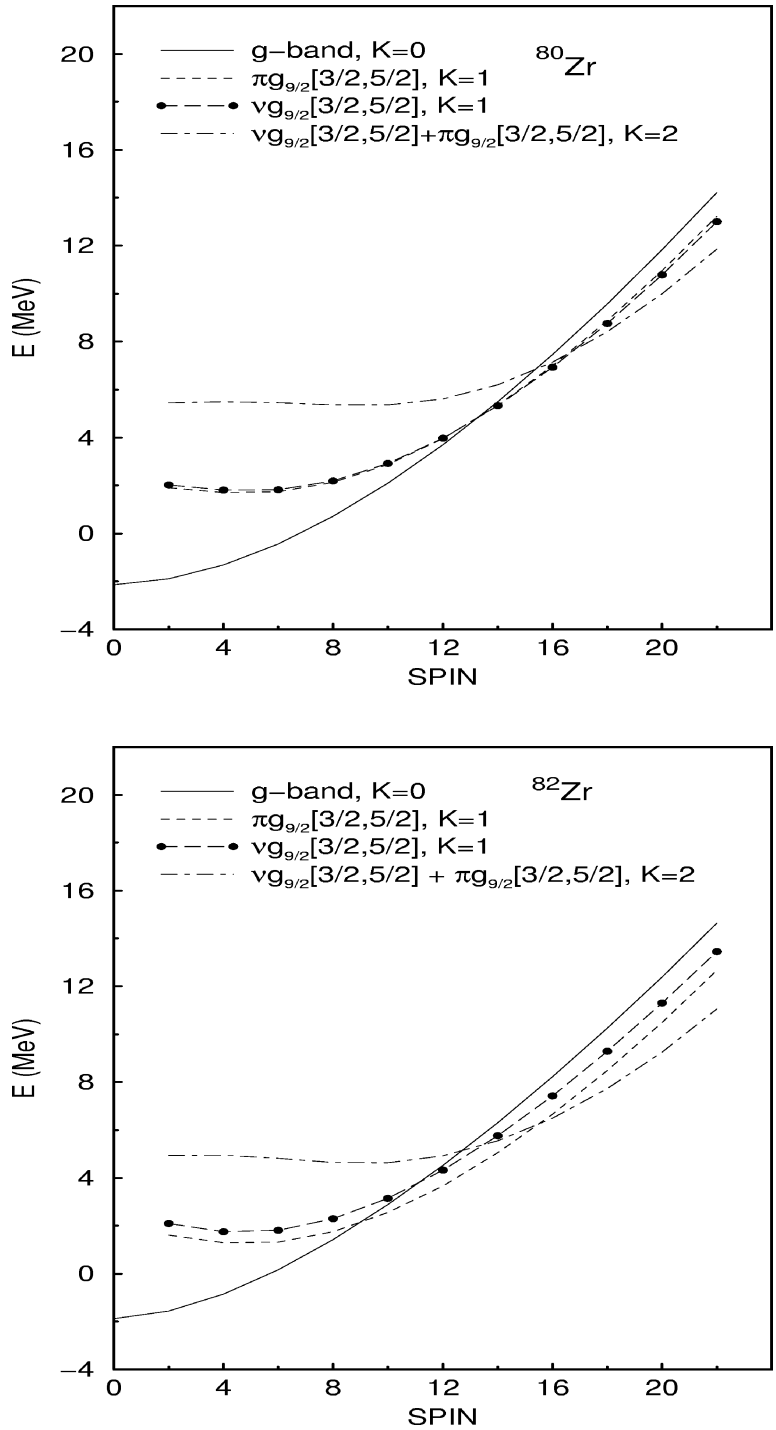

Fig. 3. Band diagrams for Zr isotopes.

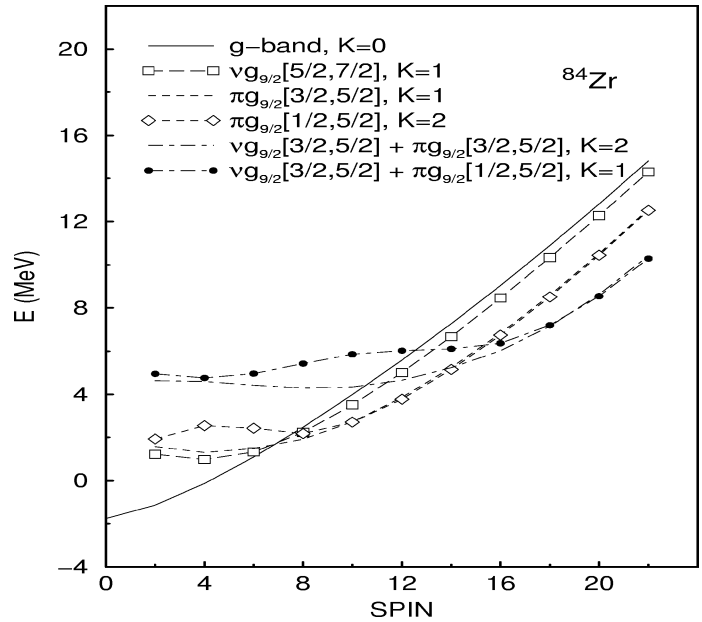

Fig. 3. —continued.

to explain the underlying physics. It should be noted that only a few of the most important configurations are plotted in the band diagrams, although many more are included in the calculations.

While most of the calculations [11,25] for the mass-70–80 nuclei at low frequency show two minima — one corresponding to a deformed prolate shape and the other to an oblate shape, very few nuclei have been found experimentally to have a collective oblate band. In fact, one such rare example is ^{68}Se, where a collective oblate band has been found in a very recent work [26]. For collective rotation perpendicular to the symmetry axis, oblate shape has least moment of inertia compared to any other shapes. This makes the rotational oblate band energetically unfavoured, unless low-lying state of oblate shape is very tightly bound (a deep minimum in potential energy surface). Hence, it is difficult to measure a collective oblate band in most of the cases. However, it is highly desirable to test the predictive power of the PSM based on an oblate mean field. For this purpose, calculations for the oblate bands in ^{68}Se and ^{74}Kr are described in the last subsection.

3.1. Kr isotopes

The proton-rich Kr-isotopes depict a variety of coexistence of prolate and oblate shapes in the low-spin region. For these nuclei, the low-lying states have an oblate deformation and the states above $I^{\pi} = 4^{+}$ are associated with a prolate shape.

The first experimental information on transitions in ^{72}Kr [28] was later confirmed in Refs. [29,30]. Recently, the level scheme has been extended up to $I^{\pi} = 16^{+}$ [9]. The experimental value of the transition strength is available only for $I^{\pi} = 8^{+}$. Following the

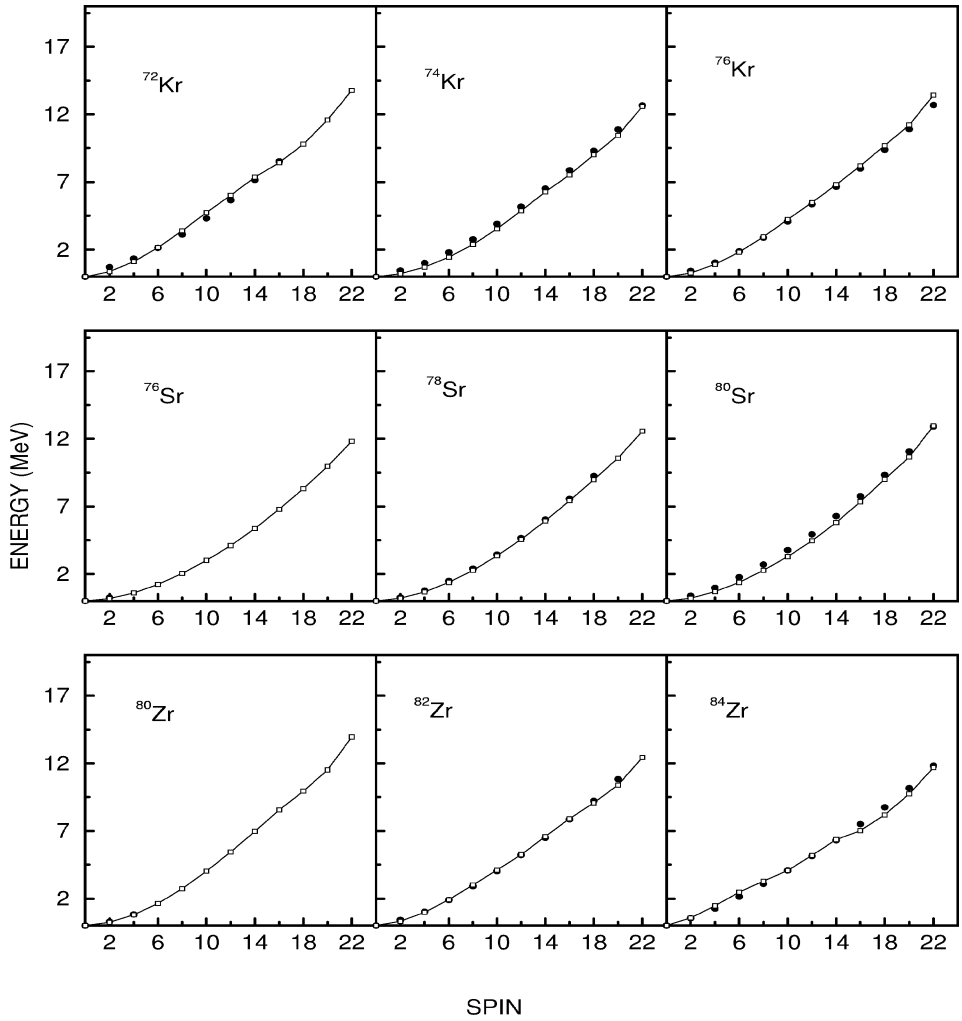

Fig. 4. Comparison of the calculated energies (open square) $E(I)$ of the yrast bands with experimental data (filled circle) for Kr, Sr and Zr isotopes. The calculated yrast bands consist of the lowest states after diagonalization at each angular momentum I.

indication in Ref. [28] that the yrast band at higher spins is prolate in nature, we have calculated the ^{72}Kr with a prolate basis deformation of $\epsilon_2 = 0.36$. As shown in the band diagram in Fig. 1, the g-band is crossed by a pair of proton 2-qp bands and a neutron 2-qp band at about $I = 10$. This gives rise to a simultaneous alignment of neutron and proton pairs. The measured energies and moment of inertia are compared with the calculated values in Figs. 4 and 5. The calculated Q_t values are shown in Fig. 6. The only data point available is in good agreement with our calculations.

Recent lifetime measurements in ^{74}Kr up to $I^\pi = 18^+$ [7] indicate a pronounced shape change induced by quasiparticle alignments. The $[440]\frac{1}{2}$, $[431]\frac{3}{2}$, $[422]\frac{5}{2}$ neutron orbitals

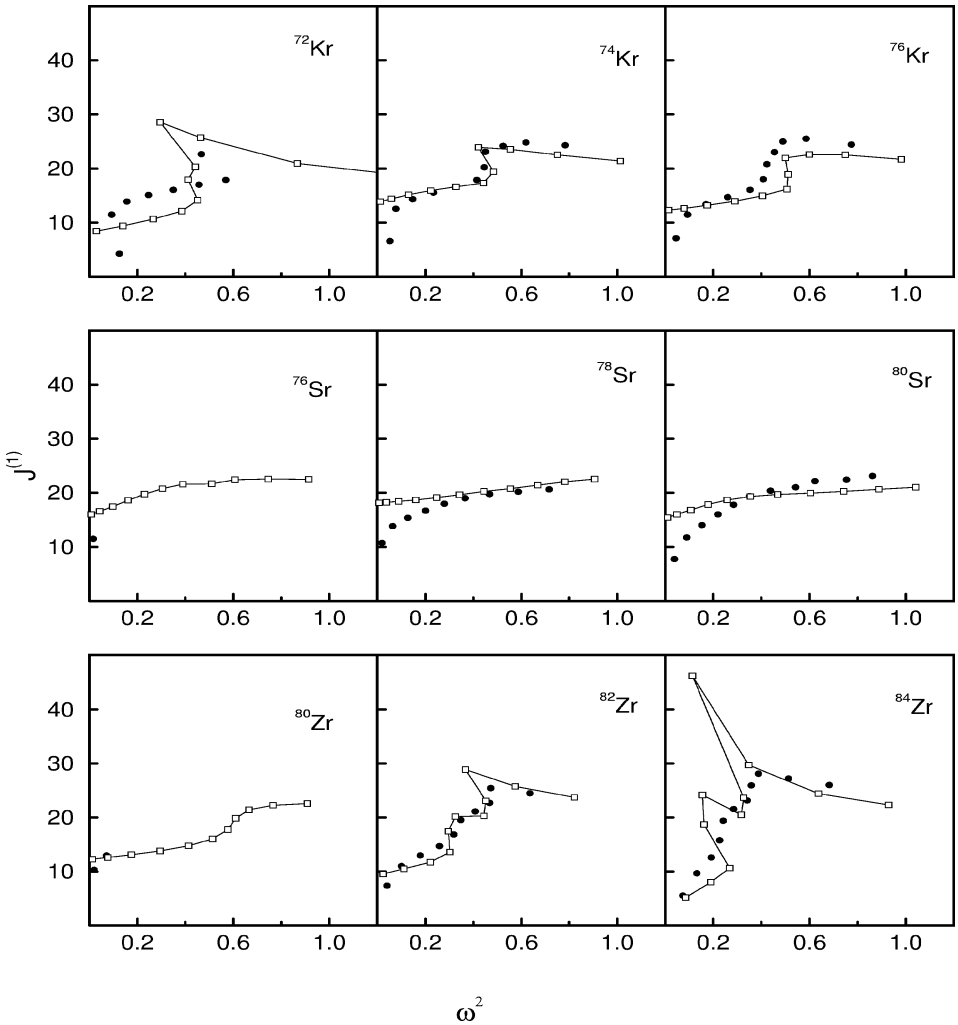

Fig. 5. Comparison of calculated moments of inertia (open square) $J^{(1)}$ with experimental data (filled circle) as a function of square of rotational frequency ω^2 for Kr, Sr and Zr isotopes. These quantities are defined as $J^{(1)} = (I - 1/2)/\omega$ and $\omega = [E(I) - E(I-2)]/2$.

and the $[440]\frac{1}{2}$, $[431]\frac{3}{2}$, $[422]\frac{5}{2}$ proton orbitals play a major role in determining the nuclear shape at the high-spin region. In order to describe the high-spin states properly, we have used the prolate deformation of $\epsilon_2 = 0.37$ in the PSM calculations for ^{74}Kr. The band diagram is shown in Fig. 1. The neutron 2-qp state $\nu g_{9/2}[3/2, 5/2]$ and two proton 2-qp states $\pi g_{9/2}[1/2, 3/2]$ and $\pi g_{9/2}[3/2, 5/2]$ cross the g-band around $I = 14$. This corresponds to the alignment of neutron and proton pairs as observed in the experiment. The yrast band, consisting of the lowest energies after diagonalization at each spin, is plotted in Fig. 4 to compare with the available experimental data. These values are also displayed in Fig. 5 in a sensitive plot of moment of inertia as a function of square of the rotational frequency.

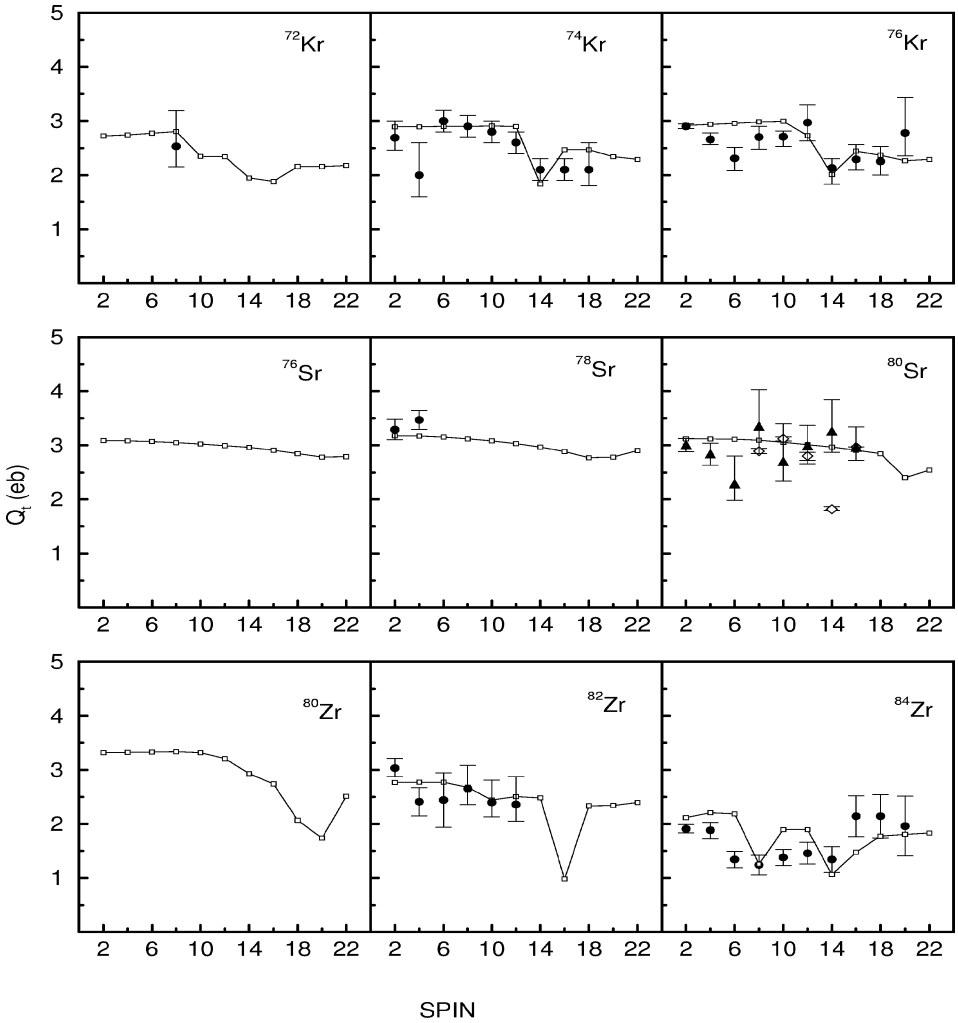

Fig. 6. Comparison of calculated transitional quadrupole moments (open square) Q_t with experimental values (filled circle) for Kr, Sr and Zr isotopes. In case of ^{80}Sr the second set [33] of experimental data (open diamond) is also plotted.

For ^{74}Kr, there is a very good agreement between the theory and experiment in both plots, except for the lowest-spin states. In Fig. 6, the Q_t values from the theory and experiment are compared. The sudden fall in the Q_t at $I = 14$, which is described correctly by our calculations, is associated with the first band crossing (see Fig. 1). Due to the occupation of the fully aligned orbitals after this band crossing, the Q_t value becomes smaller for the higher-spin states. Above $I = 18$, maximum contribution to the yrast states comes from the configuration based on the 4-qp state $\nu g_{9/2}[3/2, 5/2] + \pi g_{9/2}[1/2, 3/2]$.

The energy levels and their lifetimes in ^{76}Kr have been measured up to $I^{\pi} = 22^{+}$ along the yrast band [3,4]. Lifetime measurements indicate a large deformation in this nucleus.

A simultaneous alignment of proton and neutron pairs is observed. For this nucleus, the calculations are performed for a prolate deformation of $\epsilon_2 = 0.36$. The band diagram of ^{76}Kr is shown in Fig. 1. The g-band is crossed by the neutron 2-qp band $\nu g_{9/2}[3/2, 5/2]$ and two proton 2-qp bands $\pi g_{9/2}[1/2, 3/2]$ and $\pi g_{9/2}[3/2, 5/2]$ between $I = 12$–14. This corresponds to the simultaneous alignments of neutron and proton pairs. At higher spins, the wave function of the yrast states receives contribution from the 4-qp configurations. Though the major component of the wave function for the higher-spin states comes from the 4-qp state based on $\nu g_{9/2}[3/2, 5/2] + \pi g_{9/2}[1/2, 3/2]$ as shown in the plot, we find some amount of K-mixing with other 4-qp states leading to a nonaxial shape. The comparisons of the calculated energies and Q_t values with experimental data show good agreement as shown in Figs. 4–6. As in the ^{74}Kr case, the drop in Q_t value at spin $I = 14$ is obtained due to the occupation of the aligned states.

Although good agreement between theory and experiment for the ^{72}Kr spectrum is obtained in Fig. 4, clear discrepancy can be found in the more sensitive plot of Fig. 5. Besides the problem in the description of the moment of inertia for the lowest-spin states as in the ^{74}Kr and ^{76}Kr cases, the current calculation can not reproduce the fine details around the backbending region. For this $N = Z$ nucleus, there is an open question whether the proton–neutron pair correlation plays a role in the structure discussions [31]. In a recent study using the cranking model, it has been shown that the delayed band crossing observed in ^{72}Kr could be a signature of the proton–neutron pairing [32].

3.2. Sr isotopes

Light strontium isotopes are known to be among the well-deformed nuclei in the mass-80 region. In contrast to the Kr isotopes, data for Sr, including the most recent ones [33], do not suggest a backbending or upbending in moment of inertia (see Fig. 5). For ^{76}Sr, the only experimental work was reported in Ref. [34], where the energy of the first excited state was identified. Because of shell gap at $N = 38$, this nucleus is found to be highly deformed. We have calculated this nucleus with the basis deformation of $\epsilon_2 = 0.36$. It is found in Fig. 2 that the proton 2-qp band $\pi g_{9/2}[3/2, 5/2]$ and the neutron 2-qp band $\nu g_{9/2}[3/2, 5/2]$ nearly coincide with each other for the entire low-spin region, and cross the g-band at $I = 14$. Just above $I = 16$, the 4-qp band based on the configuration $\nu g_{9/2}[3/2, 5/2] + \pi g_{9/2}[3/2, 5/2]$ crosses the 2-qp bands and becomes the lowest one for higher spins. However, both of the first and the second band crossings are gentle with very small crossing angles. Therefore, the structural change along the yrast band is gradual, and the yrast band obtained as the lowest band after band mixing seems to be unperturbed. This is true also for the isotopes ^{78}Sr and ^{80}Sr as we shall see below. Thus, although band crossings occur in both of the Kr and Sr isotopes, smaller crossing angle results in a smooth change in the moments of inertia in Sr, and this picture is very different from what we have seen in the Kr band diagrams in Fig. 1, where sharper band crossings lead to sudden structure changes.

Ref. [35] reported the positive parity yrast cascade in ^{78}Sr up to $I^\pi = 10^+$. Their measurement of the lifetimes of the first two excited states indicate the E2 transition

strengths of more than 100 Weisskopf units. Refs. [36,37] extended this sequence up to $I^\pi = 22^+$. A broad band crossing was observed around $I = 12$ and two bands in ^{78}Sr seem to interact strongly over a wide range of spin states. To study these effects, the band energies are calculated for ^{78}Sr, assuming a prolate deformation $\epsilon_2 = 0.36$. As shown in the band diagram of ^{78}Sr in Fig. 2, the band based on the proton 2-qp state occupying $[431]\frac{3}{2}$ and $[422]\frac{5}{2}$ orbitals crosses the g-band at $I = 12$ at a very small angle. This implies a smooth structure change in the yrast band and explains the gradual alignment behavior as observed in the experiment. In fact, the neutron 2-qp band based on $[431]\frac{3}{2}$ and $[422]\frac{5}{2}$ orbitals contribute to the yrast levels between $I = 14$ to 18. The calculated energies and moment of inertia are compared with the experimental data in Figs. 4 and 5. In Fig. 6, the calculated Q_t values show a smooth behavior with a slight decreasing trend for the entire spin region, which is in contrast to the sudden drop in the Q_t curve at $I = 14$ in its isotone ^{74}Kr. The current experimental data exist only for the lowest two states. To test our prediction, the measurements for higher spins are desirable.

In a recent experiment [33], ^{80}Sr has been studied up to $I^\pi = 22^+$ along the yrast band. To observe the shape evolution along the yrast band, the lifetime of levels up to $I = 14^+$ has been measured. At low spin, a prolate shape with $\beta_2 \approx 0.35$ has been reported [33]. Taking $\epsilon_2 = 0.34$, the band diagram of ^{80}Sr is calculated and displayed in Fig. 2. A proton 2-qp band based on $\pi g_{9/2}[3/2, 5/2]$ crosses the g-band between $I = 10$ and 12 and this corresponds to the first proton pair alignment. At higher spin values, the yrast states get contribution from a large number of 4-qp configurations with different K-values (these bands are not shown in Fig. 2). The calculated spectrum is compared with data in Figs. 4 and 5. The agreement is satisfactory. In particular, the smooth evolution of moments of inertia is reproduced in Fig. 5. Two sets of measured Q_t values [33,37] are compared with our calculations. The pronounced fluctuations in the Q_t values from the early experiment [37] have been removed by the new measurement in Ref. [33]. However, our calculation does not reproduce the newly measured Q_t at $I = 14$.

3.3. Zr isotopes

The self-conjugate isotope ^{80}Zr was studied up to $I^\pi = 4^+$ by the in-beam study [10]. The excitation energy of the 2^+ state indicates a large deformation for this nucleus. In Fig. 3, the band diagrams of the proton-rich Zr isotopes are shown. The band diagram of ^{80}Zr is calculated with $\epsilon_2 = 0.36$. For the positive parity band, the [431]3/2 and [422]5/2 quasiparticle states lie close to the Fermi levels of both neutrons and protons. These orbitals play an important role in determining the alignment properties in ^{80}Zr. Between $I = 12$ and 14, the proton and neutron 2-qp bands cross the ground band at the same spin. These 2-qp bands consist of two $g_{9/2}$ quasiparticles in the [431]3/2 and [422]5/2 orbitals, coupled to $K = 1$. After this band crossing, the yrast band gets maximum contribution from both of the proton 2-qp and neutron 2-qp states, as can be seen in Fig. 3. Immediately following the first band crossing, a 4-qp band crosses the 2-qp bands at $I = 16$. In the plots of moment of inertia in Fig. 5, we see that the total effect of the first and second band

crossings produces a smooth upbending. In the Q_t plots in Fig. 6, a two-step drop in the Q_t values is predicted, which is due to the two successive band crossings.

Let us now look at the $N = Z + 2$ isotope of Zr. Recently, ^{82}Zr has been studied up to $I^\pi = 24^+$ [8]. Lifetime measurements up to $I^\pi = 14^+$ along the yrast line [2,8] indicate a smaller deformation $\epsilon_2 = 0.29$ for this nuclei. The band diagram is shown in Fig. 3. Here, the 2-qp band consists of two $g_{9/2}$ quasiprotons in [431]3/2 and [422]5/2 orbitals crosses the g-band at $I = 10$. Beyond that spin, this 2-qp proton configuration contributes maximum to the yrast states up to $I = 16$, where a 4-qp band crosses the proton 2-qp band. This 4-qp configuration is made from two quasiprotons in [431]3/2 and [422]5/2 orbitals and two quasineutrons in [431]3/2 and [422]5/2 orbitals. These two separate band crossings were observed in the experiment [2,8]. As can be seen from Figs. 4 and 5, a remarkable agreement between our calculation and experimental data are obtained. The observed complex behavior of the two-step upbending in moment of inertia in ^{82}Zr is correctly reproduced. As shown in Fig. 6, for ^{82}Zr, our theory predicts a small kink at $I = 10$ in the Q_t value corresponding to the band crossing of the proton 2-qp band. At present the accuracy of the experimental values of Q_t [2,8] is not enough to confirm this kink. Up to $I = 12$, the measured transition quadrupole moments match quite well with the calculations. At spin $I = 16$, the dip in the calculated Q_t value is because of the second band crossing. A close look at the components of the wave functions of the yrast states, shows the mixing of different intrinsic states increases after the first band crossing around $I = 10$. Thus this nucleus loses the axial symmetry at higher-spin states.

For the $N = Z + 4$ isotope of Zr, the deformation is less than the lighter ones [1]. The band diagram shown in Fig. 3 is based on calculations with the basis deformation of $\epsilon_2 = 0.22$. At least two proton 2-qp bands based on $\pi g_{9/2}[3/2, 5/2]$ and $\pi g_{9/2}[1/2, 5/2]$ configurations cross the g-band at $I = 8$, corresponding to the proton alignment. After the first band crossing till $I = 14$, these two 2-qp bands lie together and continue to interact with each other. Then one finds a neutron alignment due to the lowering of a 4-qp band between spin $I = 14$ and 16. Starting from $I = 18$, two 4-qp bands nearly coincide for the higher-spin states. The calculated energies of the yrast band are compared with that of the adopted level scheme [1] in Figs. 4 and 5. In Fig. 5, one can see that the interesting pattern of experimental moment of inertia in ^{84}Zr has been qualitatively reproduced although our calculation exaggerates the variations in the data. To see the shape evolution up to high spins, the experimental transition quadrupole moments are compared with the calculated values in Fig. 6. The measured Q_t values for ^{84}Zr [1] show different behavior from those of the neighboring even–even nuclei with an increasing trend after the second band crossing. Though the calculated values of Q_t at higher spins are lower than the experimental data, the qualitative variation is well reproduced.

The only experiment that measured g-factors has recently been performed for ^{84}Zr [24]. Though, there are big uncertainties, the three data points suggest the rigid rotor value Z/A. As we can see in the theoretical diagram given in Fig. 7, g-factors for the low-spin states in this nucleus are predicted to have a rigid body character with a nearly constant value up to $I = 6$. However, a more than doubled value is predicted for $I = 8$ with a decreasing trend thereafter. This pronounced jump in g-factor is obviously due to the proton 2-qp band

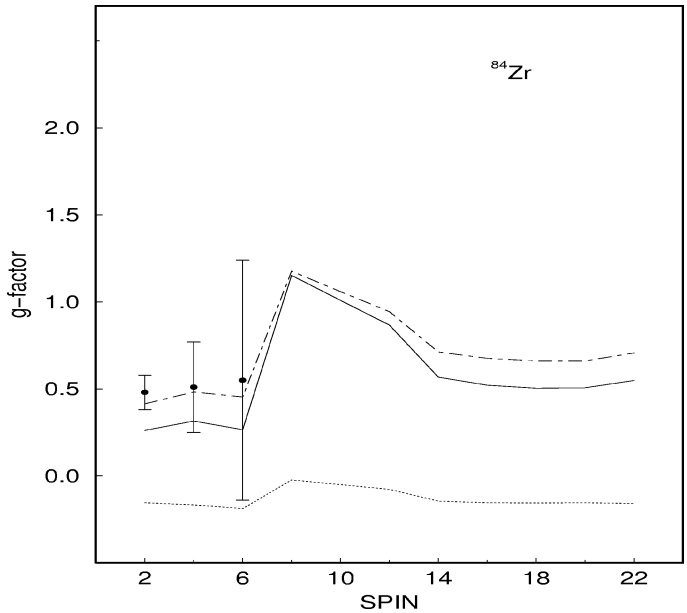

Fig. 7. Comparison of calculated gyromagnetic factors with experimental values for ^{84}Zr. For the theoretical values, dashed (dotted) line represents the g_π (g_ν) part as given in Eq. (11), and solid line gives the total g-value.

crossings at $I = 8$, as discussed above (see also Fig. 3). The wave functions of yrast states at $I = 8$ to 14 are dominated by the proton 2-qp states, thus enhancing the g-factor values. Therefore, measurement extended to higher spins in this nucleus will be a strong test for our predictions. Similar g-factor increasing at the first band crossing should also appear in the neighboring nuclei, for example in ^{82}Zr, where proton 2-qp bands alone dominate the yrast states.

3.4. Oblate bands in ^{68}Se and ^{74}Kr

A collective oblate band up to $I^\pi = 10^+$ has been identified in ^{68}Se [26]. Following the indication in Ref. [26] that yrast band is oblate in nature, we have calculated ^{68}Se for an oblate deformation $\epsilon_2 = -0.26$. As shown in the band diagram in Fig. 8(a), the g-band is crossed by a pair of proton 2-qp bands and a neutron 2-qp band at $I = 12$. This gives rise to a simultaneous alignment of neutron and proton pairs. This fact is supported by the available experimental data which shows no alignment up to $I = 10$ state. The measured energies are compared with the calculated values in Figs. 8(b) and 8(c). The calculated Q_t values are shown in Fig. 8(d).

TRS calculations for the ground state band in ^{74}Kr show a prominent oblate minimum at $\epsilon_2 \sim -0.24$ [7] along with the prolate minimum. The band diagram for the oblate configuration is shown in Fig. 9(a). The $[431]\frac{3}{2}$, $[422]\frac{5}{2}$, $[413]\frac{7}{2}$ neutron orbitals and $[422]\frac{5}{2}$, $[413]\frac{7}{2}$ proton orbitals play a major role in determining the structure of oblate band in ^{74}Kr. The two neutron 2-qp bands based on $\nu[5/2, 7/2]$ and $\nu[3/2, 7/2]$ cross

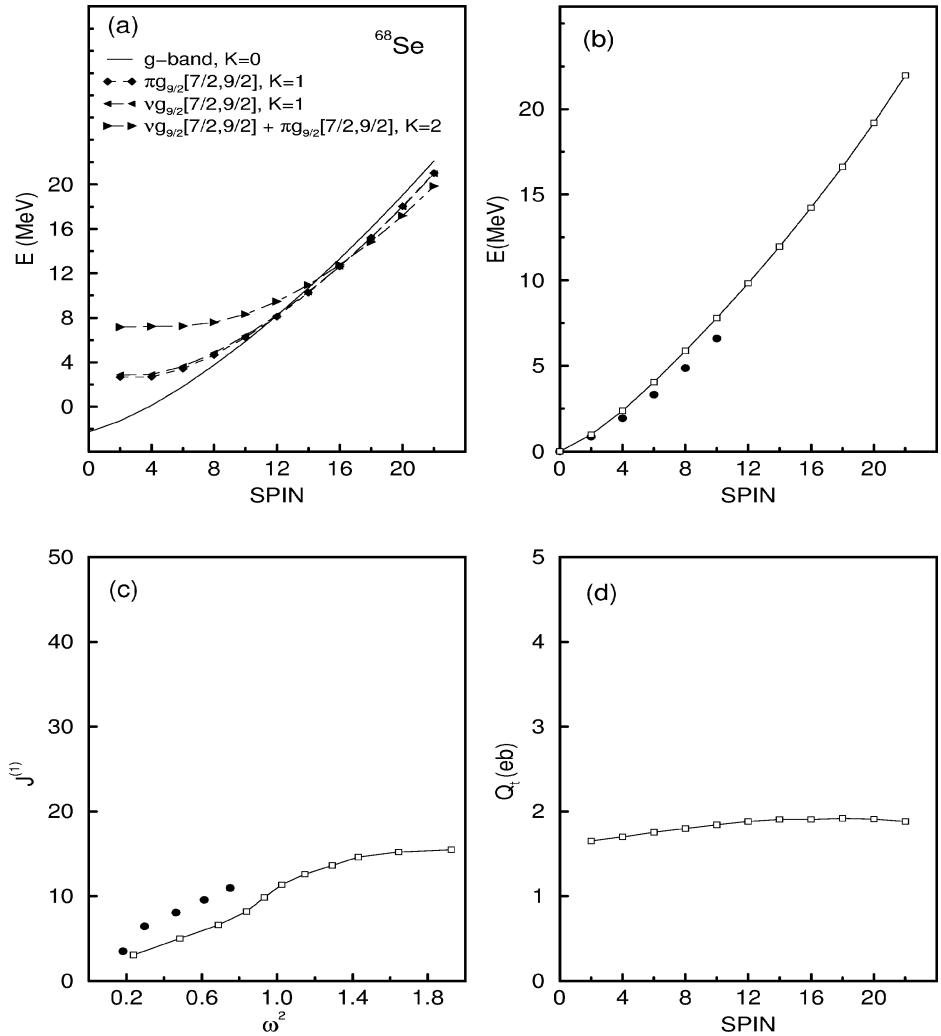

Fig. 8. (a) Band diagram for ^{68}Se with oblate deformation. Comparison of experimental (filled circle) and calculated (open square) (b) energies, (c) moment of inertia $J^{(1)}$ and (d) transition quadrupole moments Q_t for the oblate configuration in ^{68}Se.

g-band at $I = 10$. On the other hand, 2-qp proton band never becomes energetically most favourable. However, the 4-qp state $\nu[5/2, 7/2] + \pi[5/2, 7/2]$ crosses the 2-qp neutron band at $I = 18$. Thus, in case of oblate shape for ^{74}Kr one expects to see two separate alignments for neutron and proton pairs at $I = 10$ and 18, respectively. This picture is quite different from that of prolate deformation in ^{74}Kr, where the present calculation predicts a simultaneous alignment of neutron and proton pairs in agreement with the experimental results. The calculated energies for the oblate band are shown in Figs. 9(b) and 9(c). The transition quadrupole moments Q_t are plotted in Fig. 9(d). Unfortunately, no experimental data for oblate band in ^{74}Kr are available to compare with the calculations.

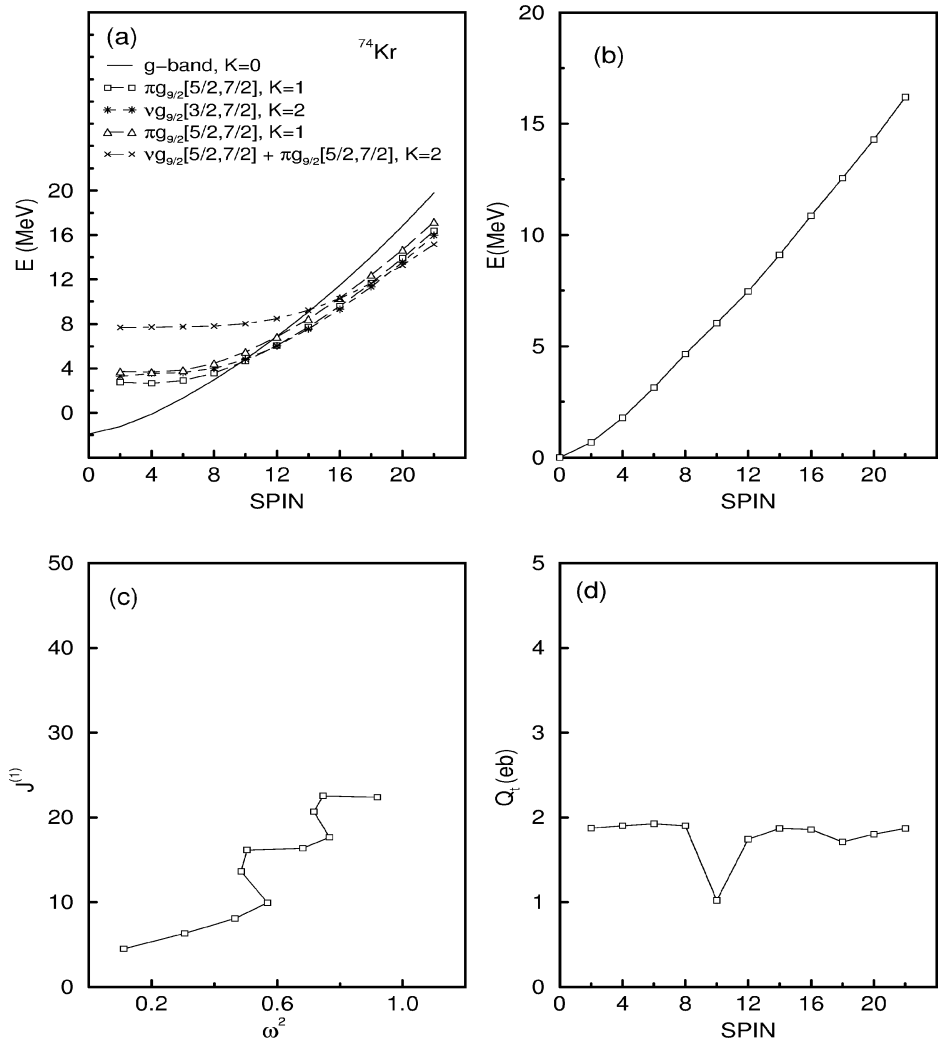

Fig. 9. (a) Band diagram for ^{74}Kr with oblate deformation. Calculated (open square) (b) energies, (c) moment of inertia $J^{(1)}$ and (d) transition quadrupole moments $Q_{\rm t}$ for the oblate configuration in ^{74}Kr are plotted.

4. Conclusion

The study of the proton-rich mass-80 nuclei is not only interesting from the structure point of view, but it also has important implications in the nuclear astrophysical study [38]. In this paper, we have for the first time performed a systematic study for the yrast bands of $T_z = 0$, 1 and 2 isotopes of Kr, Sr and Zr within the framework of the projected shell model approach. We have employed the quadrupole plus monopole and quadrupole pairing force in the Hamiltonian, and the major shells with $N = 2$, 3 and 4 have been included for the configuration space.

The proton-rich mass-80 nuclei exhibit many phenomena that are quite unique to this mass region. The structure changes are quite pronounced among the neighboring nuclei and can be best seen in the sensitive plot of Fig. 5. For the Kr nuclei, a clear backbending is observed for all the three isotopes, while for the Sr isotopes no backbending is seen. However, the Zr nuclei exhibit both the first and the second upbends. The transition quadrupole moments show corresponding variations. For these variations, we have obtained an overall qualitative and in many cases quantitative description. These variations can be understood by the mixing of various configurations of the projected deformed Nilsson states. In particular, they are often related to band crossing phenomenon.

Despite the success mentioned above, our calculations fail to reproduce states at very low spins, as can be clearly seen in the moment of inertia plot of Fig. 5 and the Q_t plot of Fig. 6. The present model space which is constructed from the intrinsic states with a fixed axial deformation may be too crude for the spin region characterized by shape coexistence. To correctly describe the low-spin region, one needs to enrich the shell model basis. Introduction of triaxiality in the deformed basis combined with three-dimensional angular momentum projection [39] certainly spans a richer space. However, in order to study the high-spin states discussed in this paper, the current space of the triaxial PSM [39] must be extended by including multi-quasiparticle states. The other possibility is to perform an investigation with the generator coordinate method [40] which takes explicitly the shape evolution into account.

The present version of the PSM uses the simplest possible residual interactions in the Hamiltonian although it is not confined so. The quadrupole plus pairing type interaction has been widely used in the nuclear structure theory, and they have well-controlled properties. It was suggested [41] that these interactions simulate the essence of the most important correlation in nuclei, so that even the realistic force has to contain at least these components implicitly. As studied in the present paper, collective quantities such as energy levels and $B(\mathrm{E2})$ and Q_t values can be well described by the PSM with this type of interactions. Quantities like $B(\mathrm{M1})$ values and g-factors can be treated reasonably as well. However, we remark that such simple schematic forces cannot describe everything that is taking place in the many-nucleon systems and thus have to be supplemented with other types of forces whenever the necessity arises. It has become increasingly important to study quantities such as β-decay probabilities. Whether the PSM wavefunction is capable of calculating the nuclear matrix elements remains to be seen.

It has been recently suggested that the neutron–proton pairing, which is not considered in the present model, could be important in describing the high-spin properties near the $N = Z$ line. For example, it has been demonstrated that the delayed band-crossing in ^{72}Kr cannot be described using the standard mean-field Woods–Saxon approach [9] and it is essential to consider the neutron–proton pairing [32]. This is also quite evident from the present study of the PSM approach. In Fig. 1, the calculated band crossing is seen to occur at about $I = 10$, whereas the observed band crossing occurs at $I = 14$. The inclusion of the neutron–proton pairing correlations in the PSM approach is a nontrivial task, because one has to reconstruct the whole program in order to couple the neutron and proton subspaces. On the other hand, it is not yet completely clear that the observed delay in the band crossing

can be totally attributed to the neutron–proton pairing. It has been only demonstrated in a simple model study [32] and more realistic calculations are needed to make the picture clearer.

References

[1] S. Chattopadhyay, H.C. Jain, J.A. Sheikh, Phys. Rev. C 53 (1996) 100.
[2] S.D. Paul, H.C. Jain, J.A. Sheikh, Phys. Rev. C 55 (1997) 1563.
[3] C.J. Gross, J. Heese, K.P. Lieb, S. Ulbig, W. Nazarewicz, C.J. Lister, B.J. Varley, J. Billowes, A.A. Chishti, J.H. McNeill, W. Gelletly, Nucl. Phys. A 501 (1989) 367.
[4] G. Mukherjee, PhD thesis, Visva Bharati University, Santiniketan, India, 1999.
[5] C. Chandler, P.H. Regan, C.J. Pearson, B. Blank, A.M. Bruce, W.N. Catford, N. Curtis, S. Czajkowski, W. Gelletly, R. Grzywacz, Z. Janas, M. Lexitowicz, C. Marchand, N.A. Orr, R.D. Page, A. Petrovici, A.T. Reed, M.G. Saint-Laurent, S.M. Vincent, R. Wadsworth, D.D. Warner, J.S. Winfield, Phys. Rev. C 56 (1997) R2924.
[6] J. Heese, D.J. Blumenthal, A.A. Chishti, P. Chowdhury, B. Crowell, P.J. Ennis, C.J. Lister, Ch. Winter, Phys. Rev. C 43 (1991) R921.
[7] A. Algora, G. de Angelis, F. Brandolini, R. Wyss, A. Gadea, E. Farnea, W. Gelletly, S. Lunardi, D. Bazzacco, C. Fahlander, A. Aprahamian, F. Becker, P.G. Bizzeti, A. Bizzeti-Sona, D. de Acuna, M. De Poli, J. Eberth, D. Foltescu, S.M. Lenzi, T. Martinez, D.R. Napoli, P. Pavan, C.M. Petrache, C. Rossi Alvarez, D. Rudolph, B. Rubio, S. Skoda, P. Spolaore, R. Menegazzo, H.G. Thomas, C.A. Ur, Phys. Rev. C 61 (2000) 031303.
[8] D. Rudolph, C. Baktash, C.J. Gross, W. Satula, R. Wyss, I. Birriel, M. Devlin, H.-Q. Jin, D.R. LaFosse, F. Lerma, J.X. Saladin, D.G. Sarantites, G.N. Sylvan, S.L. Tabor, D.F. Winchell, V.Q. Wood, C.-H. Yu, Phys. Rev. C 56 (1997) 98.
[9] G. de Angelis, C. Fahlander, A. Gadea, E. Farnea, W. Gelletly, A. Aprahamian, D. Bazzacco, F. Becker, P.G. Bizzeti, A. Bizzeti-Sona, F. Brandolini, D. de Acuna, M. De Poli, J. Eberth, D. Foltescu, S.M. Lenzi, S. Lunardi, T. Martinez, D.R. Napoli, P. Pavan, C.M. Petrache, C. Rossi Alvarez, D. Rudolph, B. Rubio, W. Satula, S. Skoda, P. Spolaore, H.G. Thomas, C.A. Ur, R. Wyss, Phys. Lett. B 415 (1997) 217.
[10] C.J. Lister, M. Campbell, A.A. Chishti, W. Gelletly, L. Goettig, R. Moscrop, B.J. Varley, A.N. James, T. Morrison, H.G. Price, J. Simpson, K. Connell, O. Skeppstedt, Phys. Rev. Lett. 59 (1987) 1270.
[11] W. Nazarewicz, J. Dudek, R. Bengtsson, T. Bengtsson, I. Ragnarsson, Nucl. Phys. A 435 (1985) 397.
[12] K. Heyde, J. Moreau, M. Waroquier, Phys. Rev. C 29 (1984) 1859.
[13] P. Bonche, H. Flocard, P.H. Heenen, S.J. Krieger, M.S. Weiss, Nucl. Phys. A 443 (1985) 39.
[14] A. Petrovici, K.W. Schmid, A. Faessler, Nucl. Phys. A 605 (1996) 290.
[15] A. Petrovici, K.W. Schmid, A. Faessler, Nucl. Phys. A 665 (2000) 333.
[16] E. Caurier, A.P. Zuker, A. Poves, G. Martínez-Pinedo, Phys. Rev. C 50 (1994) 225.
[17] K. Hara, Y. Sun, Int. J. Mod. Phys. E 4 (1995) 637.
[18] K. Hara, Y. Sun, Nucl. Phys. A 529 (1991) 445.
[19] Y. Sun, J.L. Egido, Nucl. Phys. A 580 (1994) 1.
[20] J. Döring, G.D. Johns, M.A. Riley, S.L. Tabor, Y. Sun, J.A. Sheikh, Phys. Rev. C 57 (1998) 3912.
[21] Y. Sun, S.X. Wen, D.H. Feng, Phys. Rev. Lett. 72 (1994) 3483.
[22] J. Billowes, F. Cristancho, H. Grawe, C.J. Gross, J. Heese, A.W. Mountford, M. Weiszflog, Phys. Rev. C 47 (1993) R917.
[23] A.I. Kucharska, J. Billowes, C.J. Lister, J. Phys. (London) G 15 (1989) 1039.

[24] C. Teich, A. Jungclaus, V. Fischer, D. Kast, K.P. Lieb, C. Lingk, C. Ender, T. Hartlein, F. Kock, D. Schwalm, J. Billowes, J. Eberth, H.G. Thomas, Phys. Rev. C 59 (1999) 1943.
[25] R. Bengtsson, P. Möller, J.R. Nix, J. Zhang, Phys. Scr. 29 (1984).
[26] S.M. Fischer, D.P. Balamuth, P.A. Hausladen, C.J. Lister, M.P. Carpenter, D. Seweryniak, J. Schwartz, Phys. Rev. Lett. 84 (2000) 4046.
[27] T. Bengtsson, I. Ragnarsson, Nucl. Phys. A 436 (1985) 14.
[28] B.J. Varley, M. Campbell, A.A. Chishti, W. Gelletly, L. Goettig, C.J. Lister, A.N. James, O. Skeppstedt, Phys. Lett. B 194 (1987) 463.
[29] H. Dejbakhsh, T.M. Cormier, X. Zhao, A.V. Ramayya, L. Chaturvedi, S. Zhu, J. Kormicki, J.H. Hamilton, M. Satteson, I.Y. Lee, C. Baktash, F.K. McGowan, N.R. Johnson, J.D. Cole, E.F. Zganjar, Phys. Lett. B 249 (1990) 195.
[30] S. Skoda, B. Fiedler, F. Becker, J. Eberth, S. Freund, T. Steinhardt, O. Stuch, O. Thelen, H.G. Thomas, L. Käubler, J. Reif, H. Schnare, R. Schwengner, T. Servene, G. Winter, V. Fischer, A. Jungclaus, D. Kast, K.P. Lieb, C. Teich, C. Ender, T. Härtlein, F. Köck, D. Schwalm, P. Baumann, Phys. Rev. C 58 (1998) R5.
[31] S. Frauendorf, J.A. Sheikh, Nucl. Phys. A 645 (1999) 509.
[32] J.A. Sheikh, R. Wyss, Phys. Rev. C (in press).
[33] D.F. Winchell, V.Q. Wood, J.X. Saladin, I. Birriel, C. Baktash, M.J. Brinkman, H.-Q. Jin, D. Rudolph, C.-H. Yu, M. Devlin, D.R. LaFosse, F. Lerma, D.G. Sarantites, G. Sylvan, S. Tabor, R.M. Clark, P. Fallon, I.Y. Lee, A.O. Macchiavelli, Phys. Rev. C 61 (2000) 044322.
[34] C.J. Lister, P.J. Ennis, A.A. Chishti, B.J. Varley, W. Gelletly, H.G. Price, A.N. James, Phys. Rev. C 42 (1990) R1191.
[35] C.J. Lister, B.J. Varley, H.G. Price, J.W. Olness, Phys. Rev. Lett. 49 (1982) 308.
[36] C.J. Gross, J. Heese, K.P. Lieb, C.J. Lister, B.J. Varley, A.A. Chishti, J.H. McNeil, W. Gelletly, Phys. Rev. C 39 (1989) 1780.
[37] R.F. Davie, D. Sinclair, S.S.L. Ooi, N. Poffe, A.E. Smith, H.G. Price, C.J. Lister, B.J. Varley, I.F. Wright, Nucl. Phys. A 463 (1987) 683.
[38] H. Schatz, A. Aprahamian, J. Görres, M. Wiescher, T. Rauscher, J.F. Rembeges, F.-K. Thielemann, B. Pfeiffer, P. Möller, K.-L. Kratz, H. Herndl, B.A. Brown, H. Rebel, Phys. Rep. 294 (1998) 167.
[39] J.A. Sheikh, K. Hara, Phys. Rev. Lett. 82 (1999) 3968.
[40] K. Hara, Y. Sun, T. Mizusaki, Phys. Rev. Lett. 83 (1999) 1922.
[41] M. Dufour, A.P. Zuker, Phys. Rev. C 54 (1996) 1641.